Available online at www.sciencedirect.com
ScienceDirect
Journal of Computational Physics 221 (2007) 539–557
JOURNAL OF COMPUTATIONAL PHYSICS
www.elsevier.com/locate/jcp

A Mumford–Shah level-set approach for the inversion and segmentation of X-ray tomography data

Ronny Ramlau [a], Wolfgang Ring [b,*]

[a] *Johann Radon Institute for Computational and Applied Mathematics, Austrian Academy of Sciences, Altenbergerstrasse 69, A-4040 Linz, Austria*
[b] *Institut für Mathematik, Universität Graz, Heinrichstrasse 36, A-8010 Graz, Austria*

Received 9 September 2005; received in revised form 11 May 2006; accepted 19 June 2006
Available online 18 September 2006

Abstract

A level-set based approach for the determination of a piecewise constant density function from data of its Radon transform is presented. Simultaneously, a segmentation of the reconstructed density is obtained. The segmenting contour and the corresponding density are found as minimizers of a Mumford–Shah like functional over the set of admissible contours and – for a fixed contour – over the space of piecewise constant densities which may be discontinuous across the contour. Shape sensitivity analysis is used to find a descent direction for the cost functional which leads to an update formula for the contour in the level-set framework. The descent direction can be chosen with respect to different metrics. The use of an L^2-type and an H^1-type metric is proposed and the corresponding steepest descent flow equations are derived. A heuristic approach for the insertion of additional components of the density is presented. The method is tested for several data sets including synthetic as well as real-world data. It is shown that the method works especially well for large data noise ($\sim$10% noise). The choice of the H^1-metric for the determination of the descent direction is found to have positive effect on the number of level-set steps necessary for finding the optimal contours and densities.

MSC: 49F22

Keywords: Level set method; Shape sensitivity analysis; X-ray tomography; Active contours; Mumford–Shah functional; Inverse problems; Shape optimization

1. Introduction

In medical imaging, computerized tomography (CT) is a widely used technique for the determination of the mass density f of a sample from measurements of the attenuation of X-ray beams sent through the material along different angles and offsets. The measured data g_d are connected to the density f via the Radon Transform,

* Corresponding author. Tel.: +43 316 380 5161; fax: +43 316 380 9815.
E-mail addresses: ronny.ramlau@oeaw.ac.at (R. Ramlau), wolfgang.ring@uni-graz.at (W. Ring).

0021-9991/$ - see front matter
doi:10.1016/j.jcp.2006.06.041

$$g_d(s,\omega) = Rf := \int_{\mathbb{R}} f(s\omega + t\omega^{\perp})\,dt,$$

$(s,\omega) \in \mathbb{R} \times S^1$. To compute the density distribution f the equation $g_d = Rf$ has to be inverted. It is a well-known fact that the Radon transform is not continuously invertible e.g. as a mapping from L^2 into L^2. For this reason, regularization methods have to be used in the presence of data noise. Probably the most widely used algorithm for the inversion of tomography data is the filtered back projection method [43,38]. In principle, this algorithm combines Fourier data smoothing techniques with the application of the inverse operator R^{-1} restricted to a finite dimensional subspace of the data space. Other methods include the Algebraic Reconstruction Technique (ART) [20] and classical regularization methods as truncated singular value decomposition or Tikhonov regularization (see [19]). For a good survey on the analytical properties of the Radon transform and its inverse operator and on established reconstruction techniques we refer to [33].

In many practical applications one is not only interested in the reconstruction of the density distribution but also in the extraction of some specific features within the image which represents the density distribution of the sample. For example, the planning of surgery might require the determination of the boundaries of inner organs like liver or lung or the separation of cancerous and healthy tissue. To this end, image segmentation methods are applied – a posteriori – to the output of the inversion method. Besides region growing algorithms and other ideas based on local criteria for the classification of pixels according to their membership in a certain region, deformable interfaces (snakes, active contours, level-set techniques) have received considerable attention in image segmentation in the recent years. In the latter approaches a collection of curves (surfaces for 3-D data) is introduced and iteratively updated in such a way that finally the curves separate approximately homogenous regions. This is achieved by minimizing an energy functional which penalizes the occurrence of inhomogeneous features within the distinct regions where the separating contours are the optimization variables. Different energy functionals like e.g. elastic energy in connection with edge detectors [28,9,15,23] region based functionals [37,27,26] or Mumford–Shah like functionals [11,13,22] have been considered and different geometric models for the curves as for instance parametrized snakes [45] or level-set techniques [35,42] have been used. We refer also to the monographs [3,41] for more detailed expositions of the subject.

Segmentation methods do often fail when the image is heavily contaminated with noise. For computerized tomography, the quality of reconstruction of the density function will be limited due to the data noise, and image postprocessing [47] might be necessary before segmentation. Consequently, the procedure for extracting the contour of an object in a density image usually includes the following steps:

$$\text{data} \xrightarrow{R^{-1}} \text{density function} \rightarrow \text{image postprocessing} \rightarrow \text{segmentation}.$$

The main drawback of this approach is that the measured data are only used for the reconstruction of the density distribution f. Image postprocessing and segmentation rely only on the density and errors in the reconstruction – due to numerical problems or a wrong choice of the regularization parameters – will inevitably tamper the segmentation.

The main goal of this paper is the development of an algorithm that gives simultaneously a reconstruction and a segmentation directly from the measured data. To this end, we consider the Mumford–Shah like functional

$$J(f,\Gamma) = \|Rf - g_d\|^2_{L^2(\mathbb{R}\times S^1)} + \alpha|\Gamma|. \tag{1.1}$$

Here Γ is a geometric variable which represents the set of points on or across which the density distribution f is allowed to have certain singularities. The main idea using Mumford–Shah approaches is to introduce the singularity set as an additional unknown which can be chosen within an appropriate class of sets $\mathcal{G}$. For fixed Γ the density f is chosen from a function space $X(\Gamma)$ which allows singularities of a prescribed kind on or across Γ. Usually a regularization term $\|f\|^p_{X(\Gamma)}$ is added to the functional to ensure well-posedness of the minimization with respect to f. The norm $\|\cdot\|_{X(\Gamma)}$ is constructed in such a way that the occurrence of singularities on or across Γ is not penalized by $\|\cdot\|_{X(\Gamma)}$. In our approach we choose $X(\Gamma)$ as the space of functions which are piecewise constant on $\mathbb{R}^2 \setminus \Gamma$. The rather low dimension of this space automatically ensures well-posedness with respect to f. Thus, a regularization term penalizing f is not necessary. The classical Mumford–Shah functional (where the operator R in (1.1) is replaced by the identity and a penalty term acting on f is added) was originally

designed to identify the set of jump singularities of a given function and – simultaneously – to find a smooth approximation of the function away from the singularities (see [32,10,11,22]). In our case the unknown image and the data are related via the Radon transform and not via the identity. The functional (1.1) depends on the functional variable f (the density) as well as a geometrical variable Γ. A Mumford–Shah approach for the inversion of ill-poses operator equations has been used before in [4,29], where the problem of deblurring of a given image is considered. In these papers, the Radon transform in (1.1) is replaced by a convolution operator with a smoothing (possibly unknown) kernel. In [4] an Ambrosio-Tortorelli type approximation of the Mumford–Shah functional is used (see [1] for the origin of this approximation), whereas the authors [29] use a level-set based approach.

For medical applications, it is reasonable to restrict the reconstruction to densities f that are constant with respect to a partition of the body, as the tissues of inner organs, bones, or muscles have approximately constant density. For the following we assume that – for fixed Γ – the density f is constant on each connected component of $D\backslash\Gamma$, where D denotes the domain of definition of f. The geometrical variable Γ then denotes a collection of closed curves that describe the boundaries of the regions where the function is constant, and $|\Gamma|$ is the sum of the lengths of all these curves. In our work, we extend the classical piecewise constant Mumford–Shah functional as already considered by Mumford and Shah [32] and by Chan and Vese [11] in the level-set context to the situation where the identity operator is replaced by the Radon transform R. In fact, our approach has much im common with the Chan–Vese model and the analysis and implementation of our method can be performed along the same lines as for the Chan–Vese model. Replacing the identity I by R, however, yields a more complicated optimality system for the piecewise constant function values of the density and requires more involved techniques for the shape sensitivity analysis.

By minimizing the Mumford–Shah functional (1.1), the first term on the right hand side of (1.1) ensures that the reconstruction for the functional parameter f is close enough to a solution of the equation $Rf = g$, whereas the term $\alpha|\Gamma|$ controls the length of the boundary of the partition of the image. Consequently, if the regularization parameter is chosen properly, we obtain both a reconstruction for the density f and a segmentation of the image, represented by the curves Γ, directly from the data g_d.

The main difficulty in using a Mumford–Shah approach lies in the different structure of the geometric variable (the singularity set) and the functional variable (the reconstruction) which cannot be easily treated in a straight forward way within the framework of nonlinear optimization. Usually either the geometrical variable is eliminated – leading to phase field like formulation with non-convex cost functionals for the functional variable [6,10] – or the functional variable is eliminated and the problem is reduced to a shape optimization problem [12,46,22]. Here, we follow the second approach, i.e. in

$$\min_{f,\Gamma} J(f,\Gamma), \tag{1.2}$$

we first minimize with respect to f and we denote the corresponding solution by $f(\Gamma)$. In a second step the reduced functional

$$\widehat{J}(\Gamma) = J(f(\Gamma),\Gamma) \tag{1.3}$$

is minimized with respect to Γ. The proposed algorithm uses a preconditioned shape gradient of $\widehat{J}(\Gamma)$ for the construction of a descent direction for the functional. From the point of view of algorithmic innovation the introduction of a preconditioner which is related to a Newton type descent direction for the geometric regularization term $\alpha|\Gamma|$ is one of the major issues of our paper. The preconditioned gradient direction produces smoother intermediate geometries and allows to use larger step sizes. It is also shown experimentally that, in the preconditioned formulation, the regularizing effect of the length term $\alpha|\Gamma|$ is not nullified by the possible instability of the time-stepping procedure due to the choice of too large time-steps, as it can be the case for the L^2-gradient descent.

The update of the geometry is done using the level set methodology. The idea to combine level set and shape sensitivity techniques for the solution of inverse problems was, to our knowledge, first used in [40]. Other level-set based methods for inverse problems involving shapes were considered in [30,25,36,5,8,24,14,18,17] and others.

We also address the problem of topology changes during the propagation of the interface Γ towards a minimum of (1.3). Although it is possible in the level set context for one region Ω with boundary Γ to split into two regions, and, vice versa, for two regions to merge into one, it is well known that it is usually not possible to create new regions inside already existing ones. Based on the functional gradient of (1.1) we propose a method that generates a new component of the partition of the image at locations where it is beneficial to do so. With this, we can avoid local minima at which the algorithm otherwise would get stuck.

In the last section we provide some reconstructions/segmentations for synthetic as well as for real data. It turns out that our method works particularly well if the data are very noisy. In this case, we obtain even better reconstructions for the functional parameter than standard regularization methods. The method is compared with a Tikhonov regularization approach with a total variation regularization term. Numerical studies comparing different parameter choices are presented.

2. A piecewise constant Mumford–Shah functional for X-ray tomography

Suppose we are given noisy data $g_d : \mathbb{R} \times S^1 \to \mathbb{R}$ of the Radon transform of an unknown density $f : D \subset \mathbb{R}^2 \to \mathbb{R}$, i.e.

$$g_d(s,\omega) \sim Rf = \int_{\mathbb{R}} f(s\omega + t\omega^{\perp})\,dt. \tag{2.1}$$

Moreover, we assume that the density data f are piecewise constant on an (unknown) partition of the image domain D, i.e. we assume that f is a feasible density if there exists a finite collection of closed curves $\Gamma \subset D$ such that f is constant on every connected component of $D\backslash\Gamma$. We point out already at this point that we shall use a level-set technique to represent the bounding curves Γ, i.e. we assume that $\Gamma = \{\mathbf{x} \in D : \phi(\mathbf{x}) = 0\}$ with a level set function $\phi : D \to \mathbb{R}$. The choice of level-sets for the description of Γ automatically renders certain topological configurations (triple junctions, crossing branches) as unfeasible or at least as very singular. The precise topological requirements on Γ will be given later.

Let $\mathcal{G}$ denote the set of all (feasible) finite collections of closed curves. For every $\Gamma \in \mathcal{G}$ let $\{\Omega_i^{\Gamma}\}_{i=1}^{n(\Gamma)}$ denote the set of all connected components of $D\backslash\Gamma$. We define

$$PC(D \setminus \Gamma) = \left\{ \sum_{i=1}^{n(\Gamma)} f_i \chi_{\Omega_i^{\Gamma}} : f_i \in \mathbb{R} \right\} \subset L^2(D), \tag{2.2}$$

where χ_{Ω} denotes the characteristic function of the set Ω.

We want to find simultaneously the singularity set Γ and the density function $f \in PC(D\backslash\Gamma)$ such that the Radon transform of f fits the given data g_d best possible in a least-squares sense. We therefore consider the Mumford–Shah like functional

$$J(f,\Gamma) = \|Rf - g_d\|^2_{L^2(\mathbb{R}\times S^1)} + \alpha|\Gamma|, \tag{2.3}$$

where $|\Gamma|$ is the one-dimensional Hausdorff measure of Γ. Note that it is not necessary to add a regularization term for f since – for fixed Γ – the density f is an element in the finite (usually low) dimensional space $PC(D\backslash\Gamma)$. It follows that the identification of f from g_d for fixed Γ is well-posed. However, the dependence of the functional on the geometric variable Γ might be insensitive. For this reason, the length term $\alpha|\Gamma|$ is added as a regularization term to the data fit term to guarantee well-posedness of the minimization of J with respect to Γ.

An algorithm for the minimization of the functional (2.3) which updates both variables Γ and f independently is difficult to formulate. This is mainly due to the fact that the geometry Γ defines the domain of definition of the other variable f and thus does not allow to tread f and Γ as independent. We therefore choose the following reduced formulation: for fixed Γ solve the variational problem

$$\min_{f \in PC(D\backslash\Gamma)} J(f,\Gamma). \tag{2.4a}$$

Denote the solution by $f(\Gamma)$. With that solve the *shape optimization problem*

$$\min_{\Gamma} \widehat{J}(\Gamma) \text{ with } \widehat{J}(\Gamma) = J(f(\Gamma), \Gamma). \tag{2.4b}$$

The following section deals with the numerical treatment of the reduced formulation (2.4).

3. Minimization algorithm

We now describe first in an overview and later in detail the proposed numerical approach for the minimization of the reduced functional (2.4).

Step 1: Choose an initial estimate Γ_0 for the geometry.
Step 2: For fixed Γ minimize J with respect to $f \in PC(D\backslash\Gamma)$ by solving the respective optimality system. Denote the solution by $f(\Gamma)$.
Step 3: Consider the reduced functional

$$\widehat{J}(\Gamma) = J(f(\Gamma), \Gamma). \tag{3.1}$$

Find a descent direction for the functional $\widehat{J}$ with respect to the geometric variable.
Step 4: Update Γ by moving it in the chosen descent direction according to a chosen line-search rule.
Step 5: Check for optimality:

- If the shape gradient is large go to step 2.
- If the shape gradient is small determine the derivative of the cost functional with respect to the functional variable f. If a significant maximum or minimum exists for the functional gradient introduce a new component of Γ in the vicinity of the extremum. Go back to Step 2.

We now present a detailed description of the individual steps of the algorithm.

3.1. Step 2: Solution of the optimality system with respect to f

The necessary optimality conditions for the minimum $f(\Gamma)$ of J with respect to f for fixed Γ read as

$$\partial_f J(f(\Gamma), \Gamma)h = \langle Rf(\Gamma) - g_\mathrm{d}, Rh\rangle_{L^2(\mathbb{R}\times S^1)} = 0 \tag{3.2}$$

for all $h \in PC(D\backslash\Gamma)$ where $\partial_f J$ denotes the derivative of J with respect to the first variable. The characteristic functions $\{\chi_{\Omega_i^\Gamma}\}$ form a basis in $PC(D\backslash\Gamma)$. It is therefore sufficient for the determination of $f(\Gamma)$ to claim that

$$\langle R^*(Rf(\Gamma) - g_\mathrm{d}), \chi_{\Omega_i^\Gamma}\rangle_{L^2(D)} = 0$$

for all i. With $f(\Gamma) = \sum_j f_j(\Gamma)\chi_{\Omega_j^\Gamma}$, we obtain the optimality system

$$\sum_j f_j(\Gamma) \int_{\Omega_i^\Gamma} R^*R\chi_{\Omega_j^\Gamma}\,\mathrm{d}\mathbf{x} = \int_{\Omega_i^\Gamma} R^* g_\mathrm{d}\,\mathrm{d}\mathbf{x} \tag{3.3}$$

for all connected components Ω_i^Γ of $D\backslash\Gamma$. It is known (cf. [33,39]) that the adjoint operator to the Radon transform (2.1) is given by

$$R^*g(\mathbf{x}) = \int_{\omega\in S^1} g(\langle\omega, \mathbf{x}\rangle, \omega)\,\mathrm{d}\omega, \tag{3.4}$$

where $\langle\omega, \mathbf{x}\rangle$ denotes the scalar product in $\mathbb{R}^2$ which makes sense if we identify S^1 with the unit circle in $\mathbb{R}^2$. To assemble the system matrix for (3.3) we have to calculate the quantities

$$a_{ij} = \int_{\Omega_i^\Gamma} R^*R\chi_{\Omega_j^\Gamma}\,\mathrm{d}\mathbf{x}.$$

Using (3.4) we find

$$a_{ij} = \int_{\mathbf{x}\in\Omega_i^\Gamma} \left(\int_{\omega\in S^1} \int_{t\in\mathbb{R}} \chi_{\Omega_j}(\langle\omega, \mathbf{x}\rangle\omega + t\omega^\perp)\,\mathrm{d}t\,\mathrm{d}\omega \right) \mathrm{d}\mathbf{x}.$$

With $\mathbf{y} = \langle \omega, \mathbf{x} \rangle \omega + t\omega^{\perp}$, we obtain

$$a_{ij} = 2 \int_{\mathbf{x} \in \Omega_i^\Gamma} \int_{\mathbf{y} \in \Omega_j^\Gamma} \frac{1}{|\mathbf{x} - \mathbf{y}|} \mathrm{d}\mathbf{y}\, \mathrm{d}\mathbf{x}. \tag{3.5}$$

The factor 2 in (3.5) comes from the fact that each point $\mathbf{y}$ in Ω_j^Γ corresponds to two different points (ω, t) and $(-\omega, -t)$ in $S^1 \times \mathbb{R}$. Using

$$\frac{1}{|\mathbf{y} - \mathbf{x}|} = \frac{1}{n-1} \mathrm{div}_{\mathbf{y}} \left(\frac{\mathbf{y} - \mathbf{x}}{|\mathbf{y} - \mathbf{x}|} \right) \tag{3.6}$$

in $\mathbb{R}^n$ for $\mathbf{y} \neq \mathbf{x}$ we can rewrite the inner domain integral as a boundary integral. Using (3.6) in dimension $n = 2$ we get

$$a_{ij} = 2 \int_{\mathbf{x} \in \Omega_i^\Gamma} \int_{\mathbf{y} \in \partial\Omega_j^\Gamma} \left\langle \frac{\mathbf{y} - \mathbf{x}}{|\mathbf{y} - \mathbf{x}|}, \mathbf{n}_j(\mathbf{y}) \right\rangle \mathrm{d}S(\mathbf{y})\, \mathrm{d}\mathbf{x}, \tag{3.7}$$

where $\mathbf{n}_j = \mathbf{n}_{\Omega_j^\Gamma}$ is the unit exterior normal vector to Ω_j^Γ. The remaining domain integral can be transformed into a boundary integral using

$$\left\langle \frac{\mathbf{y} - \mathbf{x}}{|\mathbf{y} - \mathbf{x}|}, \mathbf{n}_j(\mathbf{y}) \right\rangle = -\mathrm{div}_{\mathbf{x}}(|\mathbf{x} - \mathbf{y}| \mathbf{n}_j(\mathbf{y})).$$

With this we obtain

$$a_{ij} = -2 \int_{\mathbf{x} \in \partial\Omega_i^\Gamma} \int_{\mathbf{y} \in \partial\Omega_j^\Gamma} |\mathbf{y} - \mathbf{x}| \langle \mathbf{n}_i(\mathbf{x}), \mathbf{n}_j(\mathbf{x}) \rangle \, \mathrm{d}S(\mathbf{y})\, \mathrm{d}S(\mathbf{x}). \tag{3.8}$$

For the right hand side of the optimality system (3.3) we have

$$g_i = \int_{\Omega_i^\Gamma} R^* g_{\mathrm{d}}\, \mathrm{d}\mathbf{x} = \int_{\mathbf{x} \in \Omega_i^\Gamma} \int_{\omega \in S^1} g_{\mathrm{d}}(\omega \cdot \mathbf{x}, \omega)\, \mathrm{d}\omega\, \mathrm{d}\mathbf{x}. \tag{3.9}$$

Combining the above results the vector $\mathbf{f}(\Gamma) = (f_i(\Gamma))^{\mathrm{t}}$ is found as the solution to

$$A\mathbf{f}(\Gamma) = \mathbf{g} \tag{3.10}$$

where $A = (a_{ij})$ with a_{ij} given by (3.8) and $\mathbf{g} = (g_i)^{\mathrm{t}}$ with g_i given by (3.9).

3.1.1. Assembling of a_{ij}

Let us address the problem of assembling the system matrix (3.10). Let $\{\Gamma_k\}$ denote the set of all connected components of Γ. In a generic situation, where Γ – being the zero level-set of a function ϕ – has no triple junctions, each component Γ_k separates exactly two components $\Omega_{i_1(k)}^\Gamma$ and $\Omega_{i_2(k)}^\Gamma$, i.e. $\Gamma_k = \partial\Omega_{i_1(k)}^\Gamma \cap \partial\Omega_{i_2(k)}^\Gamma$. Sometimes we shall label the components of Γ by subscripts 'i, j' representing the components Ω_i^Γ and Ω_j^Γ which are separated by Γ_k. With this we have $(i, j) = (i_1(k), i_2(k))$ and we write $\Gamma_k = \Gamma_{i,j}$. Moreover let

$$c(i) = \{m : m \neq i, \partial\Omega_i^\Gamma \cap \partial\Omega_m^\Gamma \neq \emptyset\}$$

and

$$d(k) = \{i_1(k), i_2(k)\}.$$

Obviously we have $\partial\Omega_i^\Gamma = \cup_{m \in c(i)} \Gamma_{i,m}$.

Each Ω_i^Γ is a connected set on which the level set function ϕ is either everywhere positive or everywhere negative. We can therefore define

$$s(i) = -\mathrm{sign}(\phi(\mathbf{x}))$$

with some arbitrarily chosen $\mathbf{x} \in \Omega_i^\Gamma$. We also assign each $\mathbf{x} \in \Gamma$ a unit normal vector $\mathbf{n}_\Gamma(\mathbf{x})$ which, by convention, is the *exterior normal vector to the set* $\phi < 0$. We thus have

$$\mathbf{n}_{\Omega_i^\Gamma}(\mathbf{x}) = s_i \mathbf{n}_{\Gamma_{i,m}}(\mathbf{x}) \tag{3.11}$$

for every $\mathbf{x} \in \Gamma_{i,m}$. We use the abbreviations $\mathbf{n}^{i,m}(\mathbf{x}) = \mathbf{n}_{\Gamma_{i,m}}(\mathbf{x})$ and analogously $\mathbf{n}^k(\mathbf{x}) = \mathbf{n}_{\Gamma_k}(\mathbf{x})$. With this we get

$$a_{ij} = -2 s_i s_j \sum_{m \in c(i)} \sum_{n \in c(j)} \int_{\mathbf{x} \in \Gamma_{i,m}} \int_{\mathbf{y} \in \Gamma_{j,n}} |\mathbf{y} - \mathbf{x}| \langle \mathbf{n}^{i,m}(\mathbf{x}), \mathbf{n}^{j,n}(\mathbf{x}) \rangle \, \mathrm{d}S(\mathbf{y}) \, \mathrm{d}S(\mathbf{x}). \tag{3.12}$$

We assemble the coefficients a_{ij} by going in a double loop through the components Γ_k and collecting the contributions of each pair (Γ_k, Γ_l) to a_{ij}. By (3.12), the integral

$$\int_{\mathbf{x} \in \Gamma_k} \int_{\mathbf{y} \in \Gamma_l} |\mathbf{y} - \mathbf{x}| \langle \mathbf{n}^k(\mathbf{x}), \mathbf{n}^l(\mathbf{y}) \rangle \, \mathrm{d}S(\mathbf{y}) \, \mathrm{d}S(\mathbf{x})$$

contributes to each a_{ij} for which $i \in d(k)$ and $j \in d(l)$.

3.2. Step 3: Shape sensitivity analysis and construction of the descent direction with respect to Γ

To find a descent direction for $\widehat{J}$, we differentiate the reduced functional $\widehat{J}(\Gamma) = J(f(\Gamma), \Gamma)$ with respect to the geometry Γ. We use techniques from shape sensitivity calculus described e.g. in [44,16,2,22]. Rewriting the cost functional (2.3) we get

$$\begin{aligned} J(f, \Gamma) &= \left\langle \sum_i f_i R\chi_{\Omega_i^\Gamma} - g_\mathrm{d}, \sum_i f_i R\chi_{\Omega_j^\Gamma} - g_\mathrm{d} \right\rangle_{L^2(S^1 \times \mathbb{R})} + \alpha \int_\Gamma 1 \, \mathrm{d}S \\ &= \sum\nolimits_{i,j} f_i f_j \langle R\chi_{\Omega_i^\Gamma}, R\chi_{\Omega_j^\Gamma} \rangle_{L^2(S^1 \times \mathbb{R})} - 2 \sum_i \langle R\chi_{\Omega_i^\Gamma}, g_\mathrm{d} \rangle_{L^2(S^1 \times \mathbb{R})} + \langle g_\mathrm{d}, g_\mathrm{d} \rangle_{L^2(S^1 \times \mathbb{R})} + \alpha \int_\Gamma 1 \, \mathrm{d}S \\ &= 2 \sum_{i,j} f_i f_j \int_{\mathbf{x} \in \Omega_i^\Gamma} \int_{\mathbf{y} \in \Omega_j^\Gamma} \frac{1}{|\mathbf{x} - \mathbf{y}|} \, \mathrm{d}\mathbf{y} \, \mathrm{d}\mathbf{x} - 2 \sum_i \int_{\mathbf{x} \in \Omega_i^\Gamma} \int_{\omega \in S^1} g_\mathrm{d}(\omega \cdot \mathbf{x}, \omega) \, \mathrm{d}\omega \, \mathrm{d}\mathbf{x} \\ &\quad + \langle g_\mathrm{d}, g_\mathrm{d} \rangle_{L^2(S^1 \times \mathbb{R})} + \alpha \int_\Gamma 1 \, \mathrm{d}S. \end{aligned} \tag{3.13}$$

Here we used $a_{ij} = \langle R\chi_{\Omega_i^\Gamma}, R\chi_{\Omega_j^\Gamma} \rangle_{L^2(S^1 \times \mathbb{R})}$ and (3.5).

The reduced functional $\widehat{J}(\Gamma) = J(f(\Gamma), \Gamma)$ depends explicitly on Γ via the domains of integration in (3.13) and via the solution $f(\Gamma)$ of (3.3). Thus, the derivative of $\widehat{J}$ with respect to Γ formally reads as

$$\mathrm{d}\widehat{J}(\Gamma; F) = \partial_f J(f(\Gamma), \Gamma) f'(\Gamma; F) + d_\Gamma J(f(\Gamma), \Gamma; F) \tag{3.14}$$

where $\partial_f J$ denotes the derivative with respect to f for fixed Γ, $f'(\Gamma; F)$ is the shape derivative of f with respect to Γ in direction F and $d_\Gamma J(f(\Gamma), \Gamma; F)$ denotes the Eulerian derivative of J in direction F for fixed f, i.e. the derivative of $\widehat{J}$ with respect to perturbations of Γ of the form

$$\Gamma^h = \{\mathbf{x}^h = \mathbf{x} + hF(\mathbf{x})\mathbf{n}(\mathbf{x}) : \mathbf{x} \in \Gamma, \mathbf{n}(\mathbf{x}) \ldots \text{ normal vector to } \Gamma \text{ in } \mathbf{x}\}.$$

With this, the Eulerian (directional) derivative is defined as

$$\mathrm{d}J(f, \Gamma; F) = \lim_{h \to 0} \frac{1}{h} (J(f, \Gamma^h) - J(f, \Gamma)).$$

The first term on the right hand side – the derivative of the cost functional J with respect to f at $f(\Gamma)$ – vanishes due to the necessary optimality condition (3.2) which is satisfied for $f = f(\Gamma)$. The fact that the first term on the right hand side of (3.14) vanishes is always true for reduced functionals of the type (2.4). The derivative of (3.13) for fixed f with respect to Γ occurring in the various domains of integration can be found using well-known results for domain- or boundary functional of the form

$$J_\mathrm{d}(\Omega) = \int_\Omega g \, \mathrm{d}\mathbf{x} \quad \text{or} \quad J_\mathrm{b}(\Gamma) = \int_\Gamma h \, \mathrm{d}S$$

for which the differentiation rules

$$\mathrm{d}J_{\mathrm{d}}(\Omega;F)=\int_{\partial\Omega} gF\,\mathrm{d}S \quad \text{and} \quad \mathrm{d}J_{\mathrm{b}}(\Gamma;F)=\int_{\Gamma}(\langle\nabla h,\mathbf{n}\rangle+h\kappa)F\,\mathrm{d}S$$

hold. Here κ is the mean curvature of Γ. A derivation of the above results can be found e.g. in [44,16,23]. We therefore obtain

$$\begin{aligned}\mathrm{d}\widehat{J}(\Gamma;F)=2\sum_{i,j}f_if_j\left(\int_{\mathbf{x}\in\partial\Omega_i^\Gamma}\int_{\mathbf{y}\in\Omega_j^\Gamma}\frac{1}{|\mathbf{x}-\mathbf{y}|}\,\mathrm{d}\mathbf{y}F(\mathbf{x})\,\mathrm{d}S(\mathbf{x})+\int_{\mathbf{y}\in\partial\Omega_j^\Gamma}\int_{\mathbf{x}\in\Omega_i^\Gamma}\frac{1}{|\mathbf{x}-\mathbf{y}|}\,\mathrm{d}\mathbf{x}F(\mathbf{y})\,\mathrm{d}S(\mathbf{y})\right)\\ -2\sum_i f_i\int_{\mathbf{x}\in\partial\Omega_i^\Gamma}\int_{\omega\in S^1}g_{\mathrm{d}}(\omega\cdot\mathbf{x},\omega)\,\mathrm{d}\omega F(\mathbf{x})\mathrm{d}S(\mathbf{x})+\int_\Gamma\kappa(\mathbf{x})F(\mathbf{x})\,\mathrm{d}S(\mathbf{x}).\end{aligned}$$

With (3.6) and the divergence theorem we can transform the domain integrals above into boundary integrals. We get

$$\begin{aligned}\mathrm{d}\widehat{J}(\Gamma;F)=2\sum_{i,j}f_if_j\left(\int_{\mathbf{x}\in\partial\Omega_i^\Gamma}\int_{\mathbf{y}\in\partial\Omega_j^\Gamma}\left\langle\frac{\mathbf{y}-\mathbf{x}}{|\mathbf{y}-\mathbf{x}|},\mathbf{n}_j(\mathbf{y})\right\rangle\mathrm{d}S(\mathbf{y})F(\mathbf{x})\,\mathrm{d}S(\mathbf{x})\right.\\ \left.+\int_{\mathbf{y}\in\partial\Omega_j^\Gamma}\int_{\mathbf{x}\in\partial\Omega_i^\Gamma}\left\langle\frac{\mathbf{x}-\mathbf{y}}{|\mathbf{x}-\mathbf{y}|},\mathbf{n}_i(\mathbf{x})\right\rangle\mathrm{d}S(\mathbf{x})F(\mathbf{y})\,\mathrm{d}S(\mathbf{y})\right)\\ -2\sum_i f_i\int_{\mathbf{x}\in\partial\Omega_i^\Gamma}\int_{\omega\in S^1}g_{\mathrm{d}}(\omega\cdot\mathbf{x},\omega)\,\mathrm{d}\omega F(\mathbf{x})\,\mathrm{d}S(\mathbf{x})+\int_\Gamma\kappa(\mathbf{x})F(\mathbf{x})\,\mathrm{d}S(\mathbf{x}).\end{aligned}\tag{3.15}$$

It remains to arrange the terms in (3.15) according to the components $\{\Gamma_k\}$ of Γ. Note that every Γ_k appears two times as domain of integration for every integral in (3.15), once as subset of $\partial\Omega^\Gamma_{i_1(k)}$ and once as subset of $\partial\Omega^\Gamma_{i_2(k)}$ where $\{i_1(k),i_2(k)\}=d(k)$. With (3.11) we find for the first term (which we denote by $\mathrm{d}J_1(\Gamma;F)$) in (3.15):

$$\begin{aligned}\mathrm{d}J_1(\Gamma;F)&=2\sum_{i,j}f_if_j\int_{\mathbf{x}\in\partial\Omega_i^\Gamma}\int_{\mathbf{y}\in\partial\Omega_j^\Gamma}\left\langle\frac{\mathbf{y}-\mathbf{x}}{|\mathbf{y}-\mathbf{x}|},\mathbf{n}_j(\mathbf{y})\right\rangle\mathrm{d}S(\mathbf{y})F(\mathbf{x})\,\mathrm{d}S(\mathbf{x})\\ &=2\sum_{k,l}\sum_{p\in d(k)}\sum_{q\in d(l)}s_ps_qf_pf_q\int_{\mathbf{x}\in\Gamma_k}\int_{\mathbf{y}\in\Gamma_l}\left\langle\frac{\mathbf{y}-\mathbf{x}}{|\mathbf{y}-\mathbf{x}|},\mathbf{n}^k(\mathbf{y})\right\rangle\mathrm{d}S(\mathbf{y})F(\mathbf{x})\,\mathrm{d}S(\mathbf{x}).\end{aligned}$$

A symmetry argument shows that the second term in (3.15) has exactly the same form as $\mathrm{d}J_1(\Gamma;F)$. If we assemble the third integral over the components Γ_k of Γ, we likewise have to take into account the fact that each integral over Γ_k appears twice. We thus obtain

$$\begin{aligned}\mathrm{d}J(\Gamma;F)=4\sum_k\int_{\mathbf{x}\in\Gamma_k}\sum_{p\in d(k)}s_pf_p\left(\sum_l\sum_{q\in d(l)}s_qf_q\int_{\mathbf{x}\in\Gamma_k}\left\langle\frac{\mathbf{y}-\mathbf{x}}{|\mathbf{y}-\mathbf{x}|},\mathbf{n}^k(\mathbf{y})\right\rangle\mathrm{d}S(\mathbf{y})\right)\cdot F(\mathbf{x})\mathrm{d}S(\mathbf{x})\\ -2\sum_k\int_{\mathbf{x}\in\Gamma_k}\left(\sum_{p\in d(k)}s_pf_p\int_{\omega\in S^1}g_{\mathrm{d}}(\omega\cdot\mathbf{x},\omega)\,\mathrm{d}\omega\right)F(\mathbf{x})\,\mathrm{d}S(\mathbf{x})+\sum\nolimits_k\int_{\mathbf{x}\in\Gamma_k}\kappa(\mathbf{x})F(\mathbf{x})\,\mathrm{d}S(\mathbf{x}).\end{aligned}\tag{3.16}$$

A direction $F:\Gamma\to\mathbb{R}$ for which the directional derivative (3.16) is negative is called a descent direction of the functional (3.1). Since different scaling of the descent direction can always be compensated by the choice of the step-length of the optimization algorithm, a descent direction is usually normalized to $\|F\|=1$. A *steepest descent direction* is a solution to the constrained optimization problem

$$\min_F \mathrm{d}J(\Gamma;F) \quad \text{such that } \|F\| = 1. \tag{3.17}$$

Note that we have not yet specified with respect to which norm for F the steepest descent direction is found. Different norms will, in general, give different steepest descent directions.

The steepest descent direction $F^0_{\mathrm{sd}} : \Gamma \to \mathbb{R}$ with respect to the L^2-metric on Γ is found as

$$\begin{aligned} F^0_{\mathrm{sd}}(\mathbf{x}) = -4 \sum_{p\in d(k)} s_p f_p \left(\sum_l \sum_{q\in d(l)} s_q f_q \int_{\mathbf{x}\in\Gamma_k} \left\langle \frac{\mathbf{y}-\mathbf{x}}{|\mathbf{y}-\mathbf{x}|}, \mathbf{n}^k(\mathbf{y}) \right\rangle \mathrm{d}S(\mathbf{y}) \right) \\ + 2\left(\sum_{p\in d(k)} s_p f_p \int_{\omega\in S^1} g_{\mathrm{d}}(\omega\cdot\mathbf{x},\omega)\,\mathrm{d}\omega \right) - \kappa(\mathbf{x}) \end{aligned} \tag{3.18}$$

for $\mathbf{x} \in \Gamma$.

In our numerical algorithm, we suggest to employ the steepest descent direction with respect to the weighted H^1-norm

$$\|\zeta\|^2_{H^1(\Gamma)} = \|\zeta\|^2_{L^2(\Gamma)} + \frac{\nu}{2}\|\nabla_\Gamma \zeta\|^2_{L^2(\Gamma)}, \tag{3.19}$$

where ∇_Γ denotes the tangential gradient of a function defined on Γ. This choice is motivated by the second shape derivative of the regularization term $J_{\mathrm{reg}}(\Gamma) = |\Gamma|$. It is found that

$$\mathrm{d}^2 J_{\mathrm{reg}}(\Gamma;F,G) = \int_\Gamma \langle \nabla_\Gamma F, \nabla_\Gamma G\rangle \,\mathrm{d}S$$

for $\Gamma \subset \mathbb{R}^2$ (see [23,31]). The weighted H^1-norm is therefore a positive definite approximation of a semi-norm corresponding to the second order expansion of the regularization term. To find the steepest descent direction, we have to solve (3.17) with the norm constraint

$$\|F\|^2_{L^2(\Gamma)} + \frac{\nu}{2}\|\nabla_\Gamma F\|^2_{L^2(\Gamma)} = 1.$$

It is easily seen that the Karush–Kuhn–Tucker conditions imply that the steepest descent direction has the form

$$F^1_{\mathrm{sd}} = (\mathrm{id} - \nu\Delta_\Gamma)^{-1} F^0_{\mathrm{sd}}, \tag{3.20}$$

where Δ_Γ denotes the Laplace–Beltrami operator on Γ. The L^2-steepest descent direction is therefore preconditioned with an inverse elliptic operator.

3.3. Step 4: Update of the geometry via the level set technique

Using Osher's and Sethian's idea [34], propagation of an interface $\Gamma(t)$ can equivalently be expressed by a propagation law for a corresponding time-dependent level set function $\phi(t,\mathbf{x})$ where the connection between interface and level-set function is given by $\Gamma(t) = \{\mathbf{x}\in D : \phi(t,\mathbf{x}) = 0\}$. Setting F equal to a descent direction obtained above, the level set equation

$$\phi_t + F|\nabla\phi| = 0 \tag{3.21}$$

propagates ϕ and simultaneously Γ in a direction of decreasing cost functional values. For the determination of an appropriate time-step for the level-set equation we use an Armijo line search technique. The level-set equation is solved using a WENO scheme for the update (see [35] for details of the implementation).

3.4. Step 5: Inserting new components of Γ

The derivative (3.16) describes the sensitivity of the cost functional with respect to local (small) perturbation of the geometrical variable Γ. In the level-set context these perturbations can involve topology changes such as splitting or merging of components of Γ. However, the creation of a new connected component away from the current interface Γ is not a feasible perturbation of the geometry, neither in the classical setting (using perturbations of the identity or the speed method to construct perturbations), nor in the level set setting. Information whether the introduction of a new component of Γ is favorable with respect to the optimization is, therefore, not available from classical shape sensitivity analysis. Numerical experiments indicate that the evolution of the geometry Γ frequently gets stuck in local minima for which an outer contour of a large object is found, but other objects lying within the larger one are not reconstructed. In such a situation, the shape gradient (3.18) is small, but the data fit $\|Rf - g_d\|$ is not yet good enough. The data fit term describe the quality of the reconstruction in the offset-angle variables (s, ω). We are, however, interested in localized information on the quality of the reconstruction in physical domain. An indicator whether the data fit can be improved by allowing the density f to change away from the current interface Γ is the magnitude of the *functional derivative*

$$\partial_f J(f, \Gamma) = R^*(Rf - g_d). \tag{3.22}$$

The functional derivative $\partial_f J : D \to \mathbb{R}$ is large at locations where a change of the density has a large effect on the cost functional. Using this property we propose the following heuristic for the introduction of new components of Γ:

- Check if the shape gradient (3.18) is small. If this is the case:
  - Calculate the functional derivative (3.22).
  - Use a statistical test to check if $\partial_f J$ has a significant maximum or minimum.
  - If a significant maximum or minimum exists, determine locations where the values of $\partial_f J$ deviate significantly from the mean. Introduce a new component of Γ which encloses the extremum. Define a new level-set function for which the zero level-set is given by the zero level-set of the old level-set function united with the new component Γ.
  - If no significant spacial variation of $\partial_f J$ can be observed terminate the optimization.

We use the following simple test to determine whether $\partial_f J$ has a significant extremum. We first smooth $\partial_f J$ using a Gaussian filter. After that we compare the maximum and minimum value of the smoothed $\partial_f J$ on the grid points with the mean of these data. If the maximum or minimum deviates from the mean by more than a fixed multiple of the standard deviation (usually three times the standard deviation) then we introduce a new component in the vicinity of the extremum. We also make sure that the new component (a circle with center at the extremum) is small enough not to intersect any other existing component of Γ.

At this point, we briefly address the principal question of possible topology changes using level-set techniques. It is well-known that splitting and merging of domains is naturally included in the level-set methodology and can be achieved by velocity functions which are local in the sense that the velocity is given only in a neighborhood of the current interface. Although the level-set method is capable of introducing new components of the interface at locations away from the current interface by moving the graph $\{\mathbf{x}, y = \phi(\mathbf{x})\}$ of the level set function ϕ across the plane $y = 0$ at a certain (desirable) point, this can only be achieved if the speed function is defined at such points and has the tendency to push the level set function across the zero-plane. Thus, the speed function must incorporate the necessary information at which points the insertion of new components is desirable. Our approach tries to use the information in the functional derivative to introduce new components in a (discontinuous) re-initialization procedure for the level set function and restart the algorithm with the new initial level set function. An algorithm which introduces new components by continuously propagating the level set function across the zero-plane was presented in [7].

4. Numerical results

Within this section we will present some numerical results for the reconstructions from artificial and real data, as well as comparisons with other methods.

4.1. A reconstruction from artificial data

First, we report the inversion of tomography data $g(s, \omega)$ which are created synthetically using a piecewise constant density distribution f as starting point. There are five regions on which the density has a constant value, numbered 1, ..., 5 (see Fig. 1). The image for the density has a size of 320×320 pixels, and the measurements were simulated over the full circle for 319 angles and 320 offsets. The data were contaminated with 18% Gaussian noise. See Fig. 2 for the noise-free and noisy data. The reconstruction of the density distribution and its contour is shown in Fig. 3. Clearly, the reconstructed contour is very close to the original one. A comparison of the exact values of f and its reconstruction $f^{\delta}_{\alpha,\mathrm{MS}}$ in the regions 1,...,5 is given in the following table:

Region	f	$f^{\delta}_{\alpha,\mathrm{MS}}$
1	7	6.9
2	2	1.65
3	4	4.2
4	11	11.05
5	8	8.15

We conclude that, despite of the high data noise of 18%, the reconstruction quality is astonishingly good with respect to both, the contour and the density values.

In Fig. 4, the performance of the insert strategy on the artificial data set described above is illustrated. The noise-level was is set to 14%. The first row of images shows the real boundaries of the objects in the image and the current zero level-set immediately after a new component of the contour is inserted. In the second row we plot the current zero level-set atop of a color-coded plot of the functional derivative $R^*(Rf - g_{\mathrm{d}})$. Each new component is placed such that it encloses the maximum or minimum of the function $R^*(Rf - g_{\mathrm{d}})$. It is seen that the locations of new contours are correctly chosen in the vicinity of objects which have not yet been detected. The two last images in both rows show a small component which is inserted at a stage where all objects have already been found. This small contour, however, vanishes again after few iterations. The

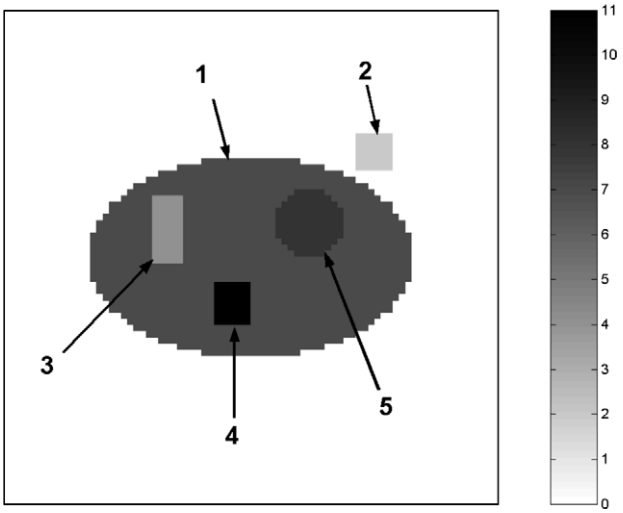

Fig. 1. Density distribution f.

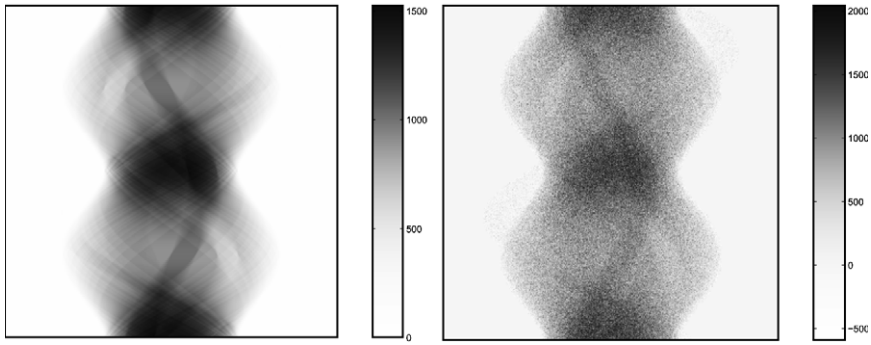

Fig. 2. Sinogram data $g(s,\omega)$ (left) and its noisy version $g_d(s,\omega)$ (right).

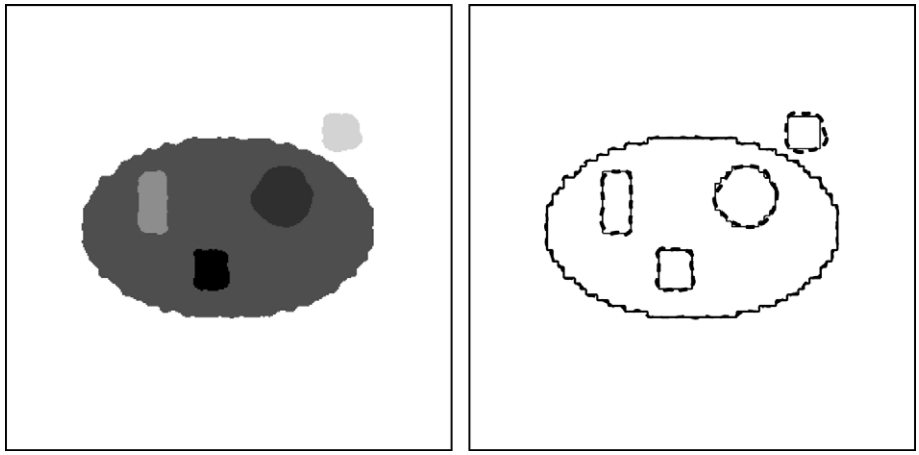

Fig. 3. (Left) Reconstructed density distribution. (Right) Contours of the true distribution (solid) and reconstructed distribution (dashed).

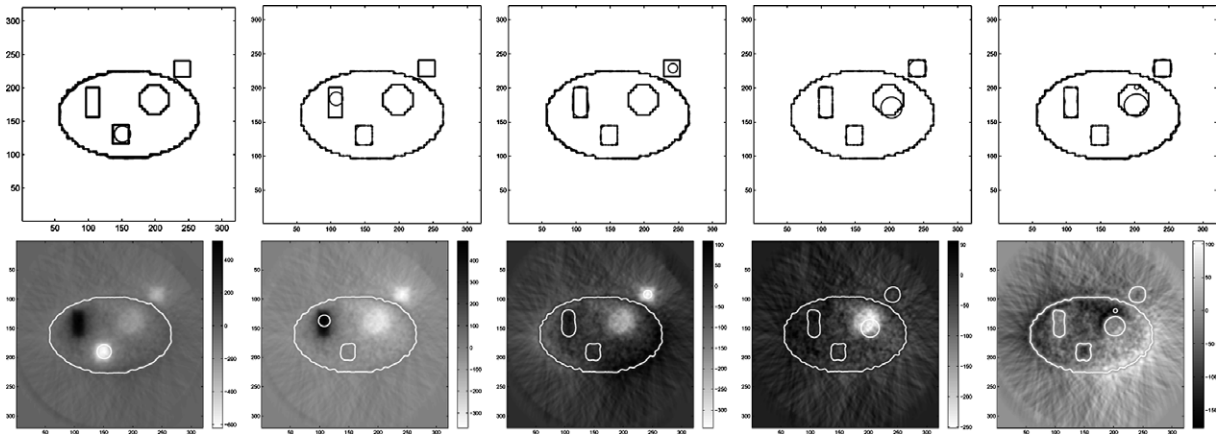

Fig. 4. Performance of the insert strategy.

algorithm is quite stable with respect to the correct detection of all objects in the image and does not produce persistent false contours.

A frequently used strategy for the detection of geometries with complicated topological structure is, to start with an initial level-set with many small components. The hope is that the small structures merge and split in the process of evolution and capture the correct topology in the end. This strategy, however, proved not to be

very successful for our Mumford–Shah model, as the numerical example in Fig. 5 shows. We start with an initial level-set with many components and many holes. After 150 iterations, the components in the center of the image have merged and correctly represent the outer shape of the large ellipse and one of the inclusions. There is no chance, however, to recover the remaining two objects inside the ellipse, since the algorithm has – at that point of the evolution – no possibility to create new contours inside existing ones. Outside the ellipse 6 objects are still present but have very low contrast with respect to the background.

4.2. Parameter studies

For the study of the influence of the parameters ν and α on the quality of the reconstruction and the performance of the numerical algorithm we chose a synthetic test example with seven objects of different size, contrast, and distance from the boundary. The exact density distribution, the noise-free and noisy sinograms are shown in Fig. 6. The noise level is 5%. With the choice of parameters $\alpha = 1$ and $\nu = 3.3$ all components could be resolved (see Fig. 7). The reconstruction of the innermost components which have the least contrast with respect to the background shows slightly oscillating contours, thus reflecting the ill-posedness of the problem in the presence of noise.

The regularization parameter α has a significant influence on the reconstruction only for values $\alpha > 10^2$. Below that value the influence of α is not significant. The algorithm, however, still converges and usually finds either all seven objects or six of them. The contours can be rather jagged. An explanation of the convergence of the algorithm for the ill-posed inversion of tomography data even if the regularization is completely switched off can be found in the fact that the degree of ill-posedness is significantly reduced by the restriction of admissible densities to the class of piecewise constant functions (2.2). Therefore the ill-posedness can express itself only in the development of very jagged contours. This, however, is suppressed to a certain degree by the inherent regularization of the level set method [21]. For large values of α the usual over-regularization

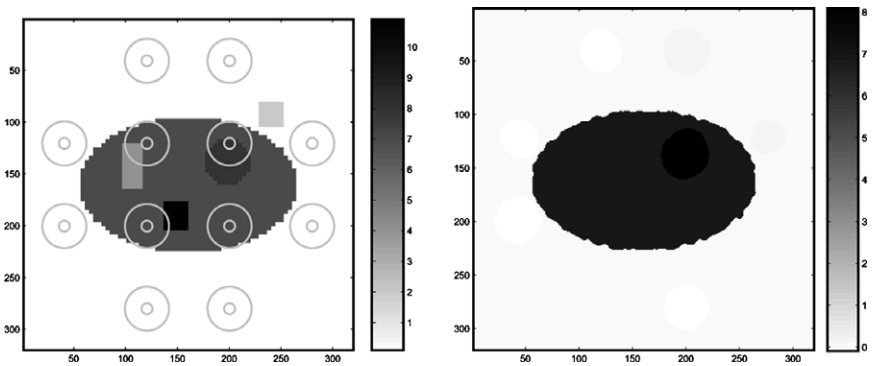

Fig. 5. Starting configuration with many components and holes, result of the reconstruction after 150 steps.

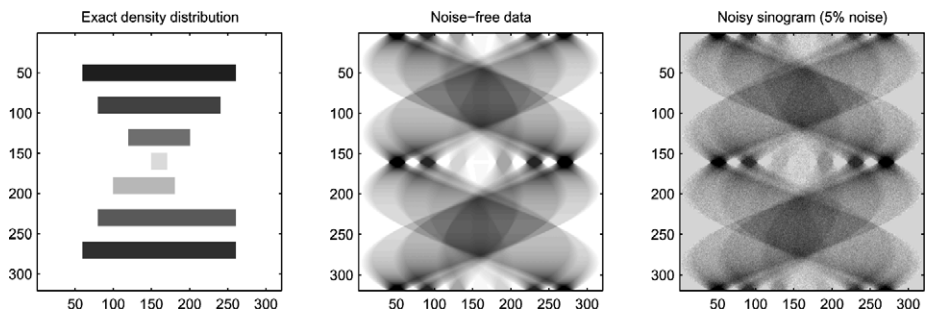

Fig. 6. Exact density distribution, exact and noisy sinograms.

effects (loss of details, over-smoothed features) become visible. A comparison for different values of α with fixed $\nu = 1$ is shown in Fig. 8.

The parameter ν, i.e. the weight which is given to the first derivative in the chosen metric (3.19) does not greatly influence the reconstruction apart form a slight regularizing effect shown in Fig. 9, where it can be seen that for $\alpha = 0$ (no penalty on the length of the contour) the resulting contour for large ν is much smoother than the contour for $\nu = 0$, with the drawback that an additional component of the density is introduced. Note that over-regularization is clearly visible in Fig. 8. For the choice $\nu = 1$ the regularizing effect of the length term is not tampered by stability problems due to a large parabolic term and an explicit time-stepping method. The greatest influence of the parameter ν is on the iteration number of the algorithm, especially if the regularization parameter α is large, i.e. the parabolic nature of the evolution problem becomes dominant. Then, preconditioning the L^2-descent direction as in (3.20) reduces the number of iterations tremendously. In Table 1 the iteration numbers are shown which are required until 6 (out of 7) objects are resolved. The insert strategy for new components was switched off since for this test example no objects are included within others and we wanted

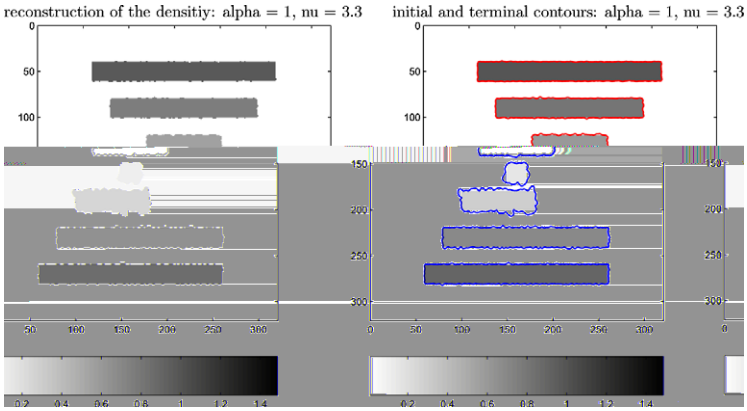

Fig. 7. Reconstruction of all seven components with an appropriate choice of parameters.

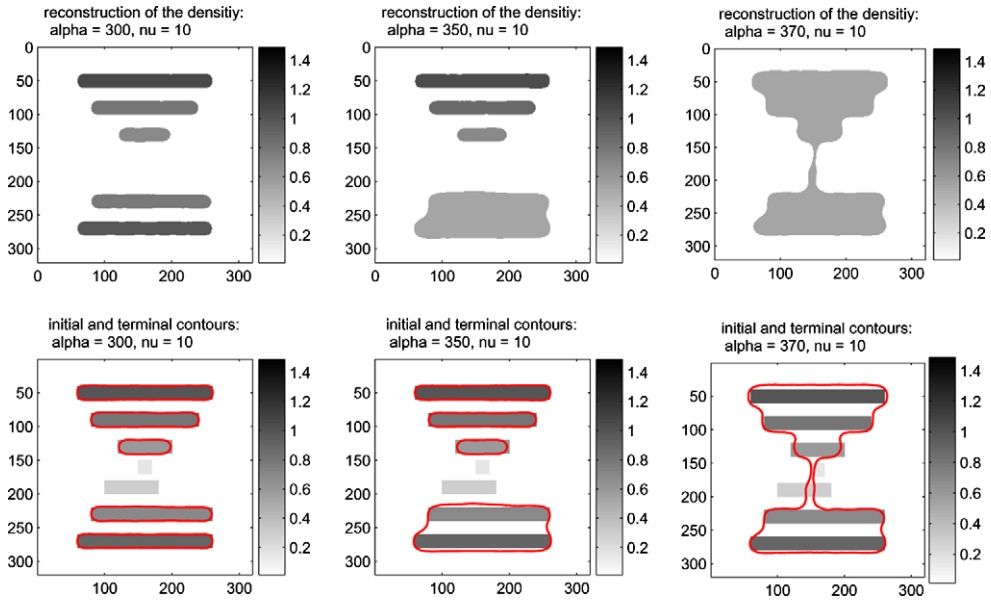

Fig. 8. Increasing over-regularization for growing α.

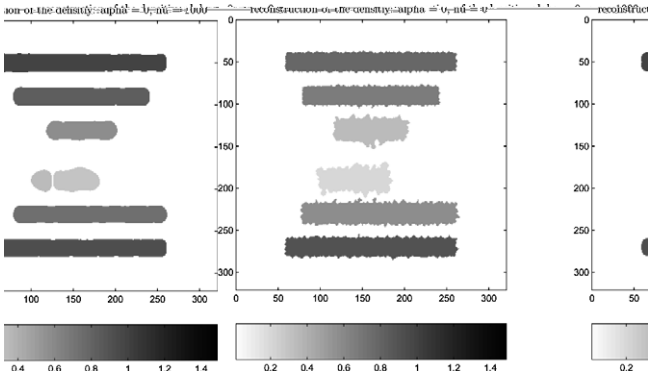

Fig. 9. Regularizing effect of the choice of the H^1-metric for $\alpha = 0$.

Table 1
Comparison of iteration numbers for different parameter choices

	$v = 10^2$	$v = 10^1$	$v = 10^0$	$v = 10^{-1}$	$v = 10^{-2}$	$v = 10^{-3}$	$v = 0$
$\alpha = 10^1$	74	52	50	–	62	68	–
$\alpha = 10^2$	105	79	134	526	1077	–	1243

Significant dependence on v for the larger value of α.

to asses the capability of the algorithm to separate objects just by splitting level-sets. Thus, the resolution of the components is achieved by pure level-set propagation starting form one contour which includes all seven objects. One typical reconstruction is shown in Fig. 10.

4.3. Mumford–Shah versus L^2-and BV-reconstructions

In this section we compare the reconstruction quality of our algorithm with results obtained by two standard algorithms: Tikhonov regularization and Bounded Variation regularization. Using Tikhonov regularization, the approximation to the solution of the equation $R(f) = g$ is computed as the minimizer of the standard Tikhonov functional

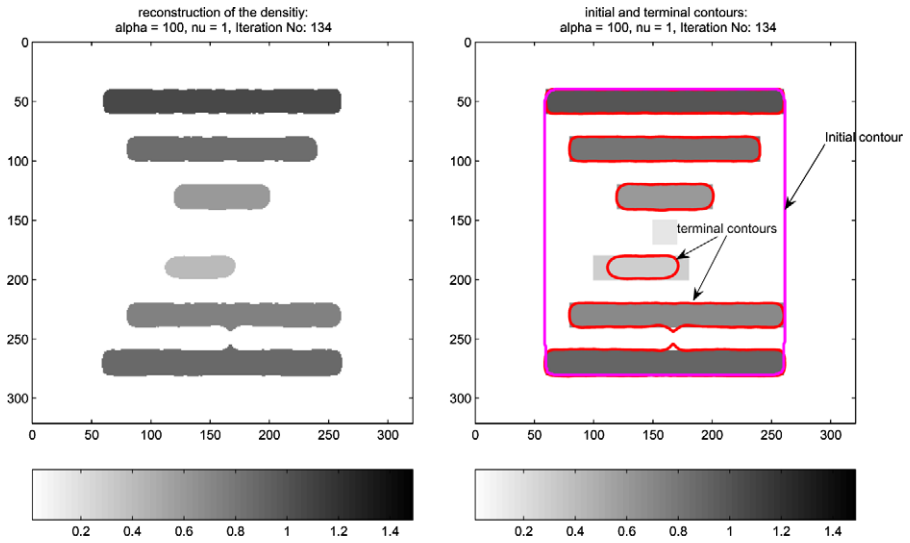

Fig. 10. Reconstruction of densities and objects after 134 iterations. Parameters $v = 1$, $\alpha = 100$.

$$f_\alpha^\delta = \arg\min_f \left\{ \|Rf - g_d\|_{L^2}^2 + \alpha \|f\|_{L^2}^2 \right\},$$

whereas the L^2 penalty term is replaced by the BV semi-norm for Bounded Variation regularization,

$$f_{\alpha,\mathrm{BV}}^\delta = \arg\min_f \left\{ \|Rf - g_d\|_{L^2}^2 + \alpha \|f\|_{\mathrm{BV}} \right\}.$$

In both cases, we chose the regularization parameter α such that the best possible reconstruction quality in the L^2 norm was reached, e.g.

$$\alpha_{\mathrm{opt}} = \arg\min_\alpha \left\{ \|f_\alpha^\delta - f\|_{L^2}, Rf = g \right\}.$$

Fig. 11 shows the reconstruction results for the noisy data from Fig. 2.

Clearly, Tikhonov regularization with L^2 penalty term gives the worst reconstruction. Some parts of the image are hardly reconstructed, e.g. region 2 almost vanishes in the reconstruction. Additionally, the image appears to be noisy, and segmentation algorithms will have difficulties to detect the contours. The BV-reconstruction is better and appears to be smoother. This is mainly due to the fact that BV regularization gives particularly good results for the class of images in $PC(D\backslash\Gamma)$ considered in this paper. Still, as the following table shows, the reconstruction quality is not as good as for our Mumford–Shah approach:

Method	Relative reconstruction error (%)
Mumford–Shah	12
BV	16
Tikhonov	26

Here, the relative reconstruction error is defined by $\|f_\alpha^\delta - f\|_{L^2} / \|f\|_{L^2}$. Moreover, the contours of the object cannot be detected as well as in the Mumford–Shah approach.

4.4. Reconstruction/segmentation from real data

We consider the reconstruction from real CT data that where collected in the context of a SPECT (single photon emission computed tomography) measurement. The SPECT data are described by the attenuated Radon transform, that depends nonlinearly on the emission function and the density distribution, but is only linear dependent on the activity function if the density function is known. Besides a SPECT scan, most SPECT scanners take CT measurements simultaneously. The data we use come from a complementary CT scan along with SPECT measurements. For our experiment, the so-called *Jaszczack torso phantom* was used. This phantom has the shape of a human torso, is filled with water and has inserts for organs like lungs or liver. Due to the simultaneous measurement process it turns out that the quality of the CT scan is much worse than for

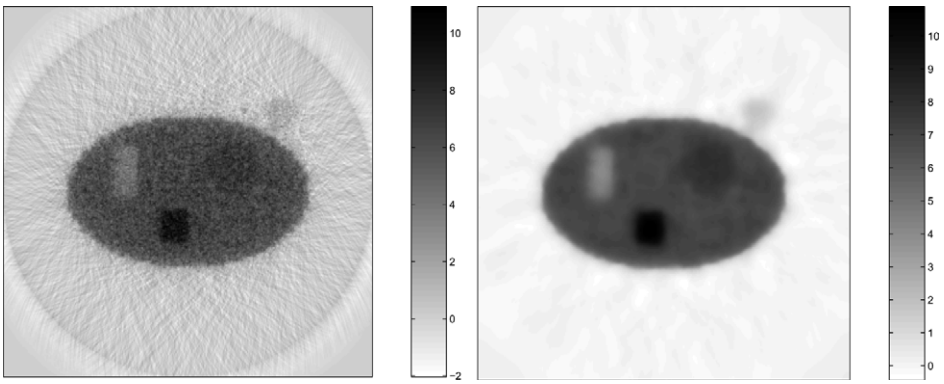

Fig. 11. Reconstructed density distributions. (Left) Tikhonov regularization with L^2 penalty term. (Right) BV regularization.

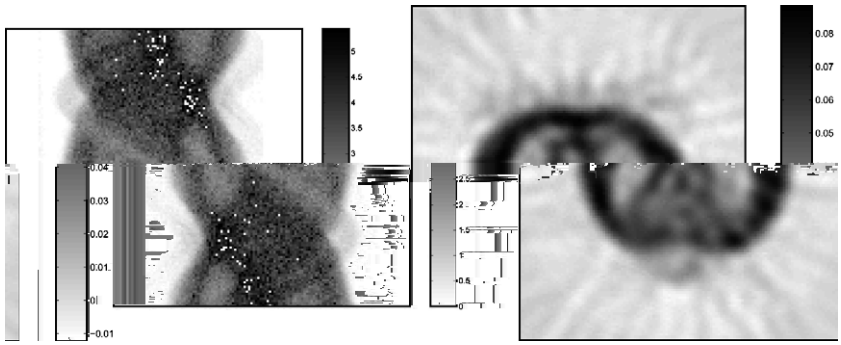

Fig. 12. Sinogram data from the Jaszczack torso phantom (l) and standard reconstruction (r).

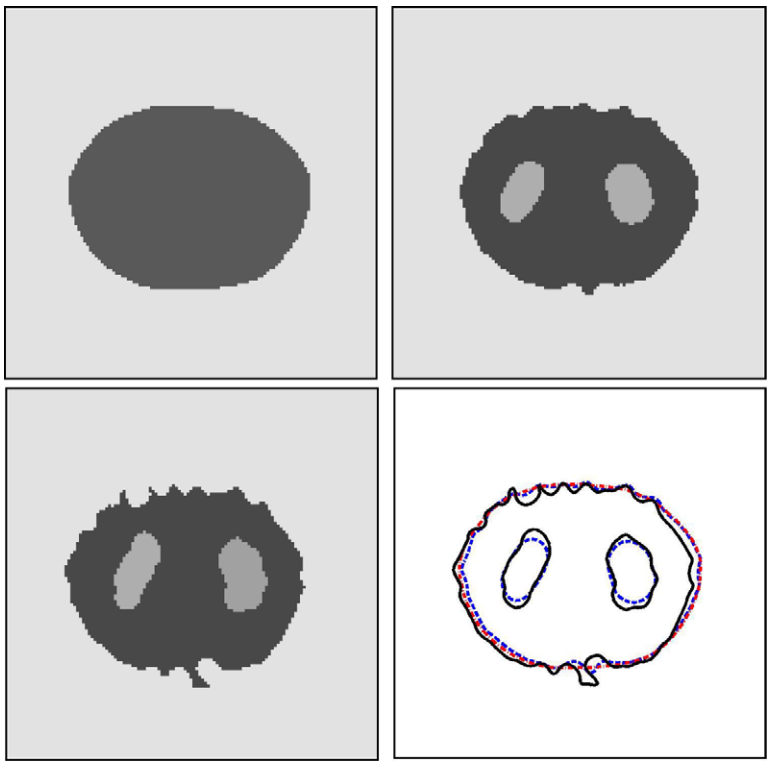

Fig. 13. Reconstructions with the Mumford–Shah algorithm for different regularization parameters: $\alpha = 0.8$(u.l.), $\alpha = 0.08$(u.r.), $\alpha = 0.008$(l.l.) and the reconstructed contours (l.r., $\alpha = 0.8$ dash-dot, $\alpha = 0.08$ dashed, $\alpha = 0.008$ solid). The color scale in the reconstructions is the same as in Fig. 12.

regular CT scanners, in the sense that the data are much noisier. See Fig. 12 for the measurement and a classical CT inversion. The data were collected over 120 angles and 128 samples, which gives a size of 128×128 for the reconstruction. The noise is estimated between 15% and 20%. The reconstruction reflects the high noise in the data. In principle, there should be only two values of the density (only the lungs have a different value), but the standard reconstruction is quite ragged, and a segmentation, e.g. for the determination of the boundary of the lungs, seems quite difficult. Fig. 13 shows the results of the reconstructions using our Mumford–Shah algorithm. If the regularization parameter α is chosen too large, the outer shape is reconstructed and smooth, but the inclusions (lungs) vanish. On the other hand, if α is to small, then the outer shape is not smooth any more. For an intermediate value of α the reconstruction is optimal in the sense that the contours are reasonably smooth and all present objects are resolved.

References

[1] Luigi Ambrosio, Vincenzo Maria Tortorelli, Approximation of functionals depending on jumps by elliptic functionals via Γ-convergence, Commun. Pure Appl. Math. 43 (8) (1990) 999–1036.

[2] Gilles Aubert, Michel Barlaud, Olivier Faugeras, Stéphanie Jehan-Besson, Image segmentation using active contours: calculus of variations or shape gradients? SIAM J. Appl. Math. 63 (6) (2003) 2128–2154 (electronic).

[3] Gilles Aubert, Pierre Kornprobst, Mathematical Problems in Image Processing, Springer-Verlag, New York, 2002, Partial differential equations and the calculus of variations, With a foreword by Olivier Faugeras.

[4] Leah Bar, Nir Sochen, Nahum Kiryati, Variational pairing of image segmentation and blind restoration, in: Pajdla, Tomás, et al. (Eds.), Computer Vision – ECCV 2004. 8th European Conference on Computer Vision, Prague, Czech Republic, May 11–14, 2004. Proceedings, Part II. Lecture Notes in Computer Science 3022, Springer, Berlin, 2004, pp. 166–177.

[5] Hend Ben Ameur, Martin Burger, Benjamin Hackl, Level set methods for geometric inverse problems in linear elasticity, Inverse Probl. 20 (3) (2004) 673–696.

[6] Andrew Blake, Andrew Zisserman, Visual Reconstruction, MIT Press Series in Artificial Intelligence, MIT Press, Cambridge, MA, 1987.

[7] M. Burger, B. Hackl, W. Ring, Incorporating topological derivatives into level set methods, J. Comp. Phys. 194 (1) (2004) 344–362.

[8] Martin Burger, Levenberg–Marquardt level set methods for inverse obstacle problems, Inverse Probl. 20 (1) (2004) 259–282.

[9] Vicent Caselles, Francine Catté, Tomeu Coll, Françoise Dibos, A geometric model for active contours in image processing, Numer. Math. 66 (1) (1993) 1–31.

[10] Antonin Chambolle, Image segmentation by variational methods: Mumford and Shah functional and the discrete approximations, SIAM J. Appl. Math. 55 (3) (1995) 827–863.

[11] T.F. Chan, L.A. Vese, Active contours without edges, IEEE Trans. Image Process. 10 (2) (2001) 266–277.

[12] T.F. Chan, L.A. Vese, A level set algorithm for minimizing the Mumford–Shah functional in image processing. in: IEEE/Computer Society Proceedings of the 1st IEEE Workshop on "Variational and Level Set Methods in Computer Vision", 2001, pp. 161–168.

[13] T.F. Chan, L.A. Vese, A multiphase level set framework for image segmentation using the Mumford and Shah model, Int. J. Comput. Vision 50 (3) (2002) 271–293.

[14] Tony F. Chan, Xue-Cheng Tai, Level set and total variation regularization for elliptic inverse problems with discontinuous coefficients, J. Comput. Phys. 193 (1) (2004) 40–66.

[15] L.D. Cohen, R. Kimmel, Global minimum for active contour models: a minimum path approach, Int. J. Comput. Vision 24 (1) (1997) 57–78.

[16] M.C. Delfour, J.-P. Zolésio, Shapes and Geometries, Society for Industrial and Applied Mathematics (SIAM), Philadelphia, PA, 2001. Analysis, differential calculus, and optimization.

[17] Oliver Dorn, Shape reconstruction in scattering media with voids using a transport model and level sets, Can. Appl. Math. Q. 10 (2) (2002) 239–275.

[18] Oliver Dorn, Eric L. Miller, Carey M. Rappaport, A shape reconstruction method for electromagnetic tomography using adjoint fields and level sets, Inverse Probl. 16 (5) (2000) 1119–1156, Electromagnetic imaging and inversion of the Earth's subsurface.

[19] H.W. Engl, M. Hanke, A. Neubauer, Regularization of Inverse Problems, Kluwer Academic Publishers, Dortrecht, 1996.

[20] R. Gordon, R. Bender, G.T. Herman, Algebraic reconstruction techniques (art) for three dimensional electron microscopy and X-ray photography, J. Theor. Biol. 29 (1970) 471–481.

[21] Eduard Harabetian, Stanley Osher, Regularization of ill-posed problems via the level set approach, SIAM J. Appl. Math. 58 (6) (1998) 1689–1706 (electronic).

[22] M. Hintermüller, W. Ring, An inexact Newton-CG-type active contour approach for the minimization of the Mumford–Shah functional, J. Math. Image Vision 20 (1–2) (2004) 19–42.

[23] Michael Hintermüller, Wolfgang Ring, A second order shape optimization approach for image segmentation, SIAM J. Appl. Math. 64 (2) (2003) 442–467.

[24] Michael Hintermüller, Wolfgang Ring, A level set approach for the solution of a state-constrained optimal control problem, Numer. Math. 98 (1) (2004) 135–166.

[25] Kazufumi Ito, Karl Kunisch, Zhilin Li, Level-set function approach to an inverse interface problem, Inverse Probl. 17 (5) (2001) 1225–1242.

[26] S. Jehan-Besson, M. Barlaud, G. Aubert, DREAM^{2}S: Deformable regions driven by an Eulerian accurate minimization method for image and video segmentation, Int. J. Comp. Vision 53 (1) (2003) 45–70.

[27] S. Jehan-Besson, M. Barlaud, G. Aubert, Video object segmentation using Eulerian region-based active contours, in: International Conference on Computer Vision, Vancouver, July 2001.

[28] M. Kass, A. Witkin, D. Terzopoulos, Snakes; active contour models, Int. J. Comput. Vision 1 (1987) 321–331.

[29] J. Kim, A. Tsai, M. Çetin , A.S. Willsky, A curve evolution-based variational approach to simultaneous image restoration and segmentation. in: IEEE International Conference on Image Processing, Rochester, NY, vol. 1, 2002, pp. 109–112.

[30] A. Litman, D. Lesselier, F. Santosa, Reconstruction of a two-dimensional binary obstacle by controlled evolution of a level-set, Inverse Probl. 14 (1998) 685–706.

[31] W. Ring, A Newton-type total variation diminishing flow, in: Proc. of the CMA conference on image processing and related inverse problems, Springer Verlag, Oslo, 2006.

[32] David Mumford, Jayant Shah, Optimal approximations by piecewise smooth functions and associated variational problems, Commun. Pure Appl. Math. 42 (5) (1989) 577–685.

[33] F. Natterer, The Mathematics of Computerized TomographyClassics in Applied Mathematics, vol. 32, Society for Industrial and Applied Mathematics (SIAM), Philadelphia, PA, 2001, Reprint of the 1986 original.
[34] Stanley Osher, James A. Sethian, Fronts propagating with curvature-dependent speed: algorithms based on Hamilton–Jacobi formulations, J. Comput. Phys. 79 (1) (1988) 12–49.
[35] Stanley J. Osher, Ronald P. Fedkiw, Level Set Methods and Dynamic Implicit Surfaces, Springer Verlag, New York, 2002.
[36] Stanley J. Osher, Fadil Santosa, Level set methods for optimization problems involving geometry and constraints. I. Frequencies of a two-density inhomogeneous drum, J. Comput. Phys. 171 (1) (2001) 272–288.
[37] N. Paragios, R. Deriche, Geodesic active regions: a new paradigm to deal with frame partition problems in computer vision, Int. J. Visual Commun. Image Represent. (Special Issue on Partial Differential Equations in Image Processing, Computer Vision and Computer Graphics, 2001), to appear.
[38] G.N. Ramachandran, A.V. Lakshminarayanan, Three-dimensional reconstructions from radiographs and electron micrographs: application of convolutions instead of fourier transforms, Proc. Natl. Acad. Sci. USA 68 (1974) 2236–2240.
[39] Andreas Rieder, Keine Probleme mit inversen Problemen, Friedr. Vieweg & Sohn, Braunschweig, 2003, Eine Einführung in ihre stabile Lösung. [An introduction to their stable solution].
[40] F. Santosa, A level-set approach for inverse problems involving obstacles, ESAIM: Control Optim. Calc. Variat. 1 (1996) 17–33.
[41] Guillermo Sapiro, Geometric Partial Differential Equations and Image Analysis, Cambridge University Press, Cambridge, 2001.
[42] J.A. Sethian, Level Set Methods and Fast Marching Methods, second ed., Cambridge University Press, Cambridge, 1999, Evolving interfaces in computational geometry, fluid mechanics, computer vision, and materials science.
[43] L.A. Shepp, B.F. Logan, The Fourier reconstruction of a head section, IEEE Trans. Nucl. Sci. NS-21 (1974) 21–43.
[44] J. Sokołowski, J.-P. Zolésio, Introduction to Shape Optimization, Springer-Verlag, Berlin, 1992, Shape sensitivity analysis.
[45] Demetri Terzopoulos, Deformable models: classic, topology-adaptive and generalized formulations, in: Geometric Level Set Methods in Imaging, Vision, and Graphics, Springer, New York, 2003, pp. 21–40.
[46] A. Tsai, A. Yezzi, A.S. Willsky, Curve evolution implementation of the Mumford–Shah functional for image segmentation, denoising, interpolation, and magnification, IEEE Trans. Image Process. 10 (8) (2001) 1169–1186.
[47] J. Weickert, Anisotropic Diffusion in Image ProcessingECMI Series, Teubner, Stuttgart, 1998.